THE JOURNAL OF PHYSICAL CHEMISTRY C
A JOURNAL OF THE AMERICAN CHEMICAL SOCIETY

pubs.acs.org/JPCC
Article

Exploring the Water-Induced Local Degradation of Metal−Organic Framework Films Using Nanoscale Infrared Spectroscopy

Marius R. Bittermann,* Sudheer Singh Rana, Michael Tovar, and Lars Heinke

Cite This: J. Phys. Chem. C 2025, 129, 16617−16623

Read Online

ACCESS | Metrics & More | Article Recommendations | Supporting Information

ABSTRACT: A plethora of applications for metal−organic frameworks (MOFs) rely on the loading of molecules into their nanoporous structures. Some MOFs, especially those containing carboxylate linkers, degrade in humid environments, detracting from their use in many applications. In the case of HKUST-1, humidity-induced hydrolysis of its Cu−O bonds can severely impair the uptake of guest molecules into its pores. However, most studies have analyzed HKUST-1 degradation in batches of crystals, while single-crystal degradation remains largely unexplored. We employ nanoinfrared spectroscopy to monitor single nanoscale HKUST-1 thin film crystals exposed to humidified gas over several days. Our results show degradation follows first-order kinetics and is accompanied by morphological changes including crack formation and the growth of large crystals of a hydrated phase. This study provides nanoscale insight into the humidity-induced degradation of MOF thin films, which can offer understanding to support long-term performance in applications such as gas separation, sensing or catalysis.

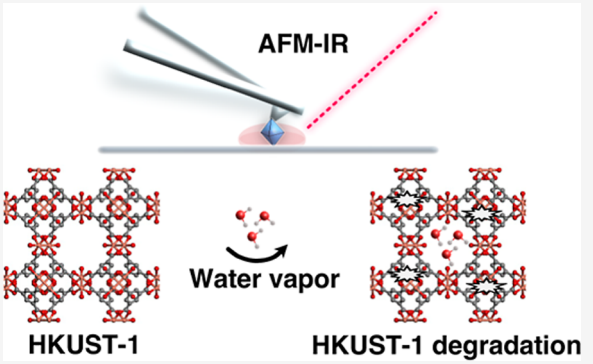

INTRODUCTION

Metal−organic frameworks (MOFs) are nanoporous, crystalline materials encompassing metal nodes connected by organic linker molecules that have risen remarkably in popularity within the last two decades.[1−3] MOFs offer flexibility in their design by combining various inorganic nodes with organic linkers, which enables precise control over their physicochemical properties, such as pore size, storage capability and thermal or chemical stability. This versatility leads to promising applications ranging from catalysis,[4] energy storage and conversion,[5,6] gas storage and separation,[7,8] chemical sensing[9,10] to biomedical applications,[11,12] including their use as nanoplatforms for antitumor research.[13] Most use cases involve the uptake of guest molecules by a host MOF structure, facilitated by their large surface area and nanoporosity. Thus, the uptake capacity of MOFs relies on retaining their structural integrity under different operating conditions. Some MOFs, however, suffer from low chemical, thermal or mechanical stability.[14] Water, for example, has been identified as a major contributor to the breakdown of the structural integrity of several MOFs.[15] This is unfortunate considering the ubiquity of water vapor in many industrial applications, for instance in CO_2 capture.[16] HKUST-1, one of the most popular and studied model MOFs,[17] is a prime example of a MOF whose susceptibility to water-induced structural breakdown hampers its widespread industrial utilization. In HKUST-1 the presence of water vapor was shown to first introduce defects on its surface,[18,19] followed by a complete collapse of its paddlewheel structure.[20−22] A direct consequence of the buildup of surface defects concerns the uptake rate of HKUST-1, which was shown to be lessened by ≈80% in mere seconds upon exposure to water vapor, while its crystal structure remains intact.[18] Prolonged exposure to water vapor was shown to induce morphological changes in HKUST-1 microscale crystals with a sharp decline in BET surface area and pore volume.[20] Infrared spectroscopy data assigned the hydrolytic breakdown to commence with the protonation of trimesic acid linkers and the coordination of water to the Cu^{2+} node.[19,20,23,24] X-ray diffraction revealed that hydrolysis of HKUST-1 in water results in the formation of new crystalline phases, including hydrated laminar structures such as $[Cu_2(BTC)(H_2O)_6]$ and $[Cu_2(BTC)(OH)(H_2O)]$.[22,25,26]

Gaining a nanoscale understanding of the interaction between water and MOFs and how it leads to their degradation is crucial, considering that most applications rely on the interaction between the MOF host structure and the guest molecules. In addition, MOF crystals can be synthesized on the nanoscale, often realized in MOF thin films,[27] which offer unique advantages in certain applications given their large surface-to-volume ratios and enhanced guest-sorption ki-

Received: May 16, 2025
Revised: August 26, 2025
Accepted: September 2, 2025
Published: September 4, 2025

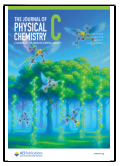

netics.[28] However, traditional vibrational spectroscopy lacks the required spatial resolution to provide insight on that scale due to the limit set by diffraction. To circumvent this limit, nanospectroscopic tools based on near-field interactions have gained popularity to study thin-films of MOFs.[29] Examples include the study of gas sorption on ZIF-8 microcrystals,[30] to track the growth of HKUST-1 thin films at different temperatures,[31] to investigate the rotor-dynamics of MOF films on the nanoscale,[32] or to probe structural defects.[33,34]

Here, we use atomic force microscopy-infrared spectroscopy (AFM-IR), a near-field technique based on the photothermal effect,[35,36] to evaluate the water-induced local degradation of single HKUST-1 nanoscale crystals. We probe the framework collapse of several individual crystals when exposed to a flow of humidified N_2 over the course of up to 60 h by following the evolution of vibrational bands associated with the framework. The combination of AFM with infrared spectroscopy allows us to demonstrate a strong correlation between the water-induced framework collapse, which follows first-order kinetics, and morphological changes in MOF thin films. We highlight that this approach provides a powerful platform for directly probing chemical and morphological transformations of MOF thin films at the nanoscale. It can be broadly applied to other MOFs to better understand their long-term stability under humid or otherwise destabilizing conditions.

METHODS

HKUST-1 Thin Film Synthesis. HKUST-1 thin film was synthesized using a layer-by-layer approach with a dipping robot.[37] First, 5 mm thin quartz substrates were cleaned by sonication in a solution consisting of ethanol, deionized water and acetic acid in a 1:1:1 ratio for 3 min. Subsequently, the substrates were further cleaned with absolute ethanol and dried with argon gas 3 times. The substrates were then functionalized using UV-Ozone for 20 min. To grow the thin films, clean substrates were dipped alternately in 1 mM ethanolic Copper(II) acetate monohydrate (Sigma-Aldrich) solution (for 5 min) and 0.2 mM ethanolic benzene-1,3,5-tricarboxylic acid (by Sigma-Aldrich) solution (for 10 min) with 2 ethanol rinses (for 1 min each) in between the dipping into the linker and metal solutions for a total of 200 cycles. 1% Milli-Q water was added to the linker solution as a modulator.[38] This procedure gave a film thickness of ≈350 nm (Figure S1). To study the dynamics of HKUST-1 degradation the samples were subjected to a flow of humidified N_2 in a glass tube using a bubbler for a total of 60 h. This technique achieved a RH > 90%. The sample was taken out of the glass tube at discrete time steps for the atomic force microscopy-infrared spectroscopy (AFM-IR) measurements.

AFM-IR Measurements. For the AFM-IR experiments, a nanoIR2s (from Bruker) coupled with a quantum cascade laser (QCL, from Daylight Solutions) was used. The QCL operated in pulsed mode and covered the wavenumber range between 1314 cm^{-1} and 1888 cm^{-1} with a wavenumber-dependent laser power averaging ∼1 mW and laser pulse width set to ≈700 ns. All measurements employed a gold-coated tip with a nominal radius of 20 nm, a free-air resonance frequency of 13 kHz and a spring constant of 0.2 N/m (PR-EX-CnIR-B-10, by Bruker). Detailed scans of 3.5 μm × 3.5 μm areas containing single crystals were measured in contact mode at 0.5 Hz per line with 350 points in both x- and y-directions. Overview scans were recorded in areas of 60 μm × 30 μm with 600 points in both x- and y-directions. Tip-induced deformation of the samples while being measured in contact mode is negligible given the low spring constant of the tip. The data was flattened during the measurement by the instrument software Analysis studio using a line fit. Overview images were additionally flattened using line-by-line polynomial fitting (degree 1) to compensate for artifacts introduced due to large height variations within the samples. For each scan line, the upper 15% of the data representing tall features were excluded from the fit. Spectra were measured at the center of each crystal in resonance-enhanced contact mode at the second contact-resonance frequency of the tip ≈145 kHz using a spectral resolution of 2 cm^{-1}. Point spectra were averaged 10 times per spot and background-corrected by dividing through the separately measured power spectrum of the laser. Crystal size was extracted using Analysis Studio software. All other data analysis was conducted using Python. For preprocessing, spectra were smoothed using a Savitzky−Golay filter with a window length of 13 and a polynomial order of 2. The surface roughness was quantified from AFM height maps as $R_a = \frac{1}{N}\sum_i^N |h_i - \bar{h}|$. For the overview images the roughness was calculated between the 2nd and 98th percentiles to compensate for sharp variations in height observed in some measurements.

X-ray Diffraction Measurements. X-ray diffraction characterization was carried out using a Bruker D8-Advance powder diffractometer (Cu K$\alpha_{1,2}$, λ = 1.5444 Å) in a θ-θ out-of-plane configuration, where the sample surface remains horizontal and the X-ray source and detector are each moved by θ. Measurements were taken with a step size of 0.02° for a total measurement time of 30 min per sample.

RESULTS

The freshly prepared HKUST-1 thin film samples are highly (mono)crystalline according to the measured X-ray diffraction (XRD) patterns, as shown in Figure 1. The strong peaks of pristine HKUST-1 at (200) and its higher-order reflection at (400) match the calculated crystallographic orientation of HKUST-1. After exposure to water vapor for 60 h new peaks at

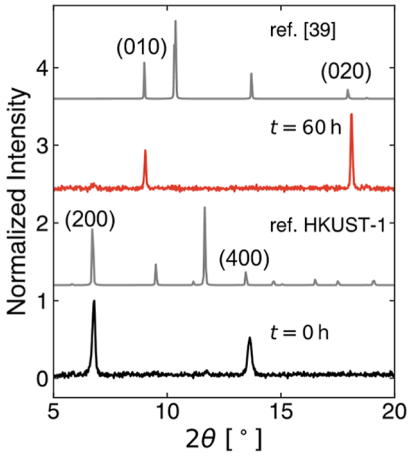

Figure 1. Normalized XRD patterns of the sample measured in its pristine state (t = 0 h) versus its degraded state (t = 60 h) compared to the reference XRD patterns of pristine HKUST-1 and $[Cu_2(OH)(BTC)(H_2O)]n{\cdot}2nH_2O$.[39] The reflections at (200) and (400) of the reference HKUST-1 sample align with the reflections observed in the measured pristine HKUST-1. In its degraded state, the two peaks observed correspond to the (010) and (020) reflections of $[Cu_2(OH)(BTC)(H_2O)]n{\cdot}2nH_2O$.

https://doi.org/10.1021/acs.jpcc.5c03355
J. Phys. Chem. C 2025, 129, 16617−16623

higher 2θ values signal a contraction in unit cell size and thus the collapse of the original HKUST-1 framework. This shift in the XRD patterns upon water-induced HKUST-1 degradation was observed before, and assigned to the formation of new crystalline phases of hydrolyzed HKUST-1.[22,25,26,39,40] Our XRD pattern suggests the phase $[Cu_2(OH)(BTC)(H_2O)]n\cdot 2nH_2O]$ (Figure 1).[39] Notably, even in its degraded state, the formed crystalline structure of the MOF thin film remains highly oriented, as evidenced by the presence of only its (010) and (020) planes.

Using atomic force microscopy-infrared spectroscopy (AFM-IR), we followed the spectral and morphological evolution of the HKUST-1 thin film on the nanoscale. Figure 2 shows AFM height images of the same position of a large 60

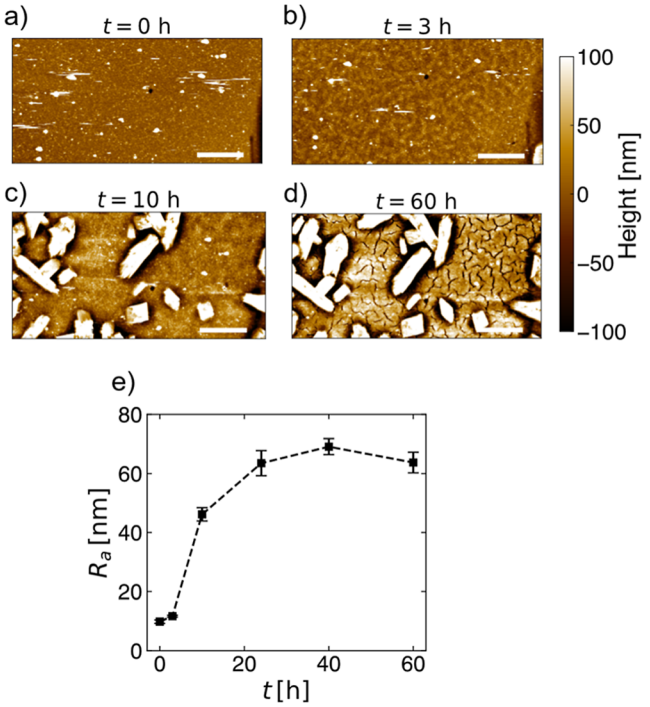

Figure 2. (a–d) AFM height images of a large area of HKUST-1 thin film in the pristine state, and after exposure to humidified N_2 for 3 h, 10 and 60 h, respectively. Scale bars are 10 μm. (e) Surface roughness R_a, calculated as $\frac{1}{N}\sum_i^N |h_i - \bar{h}|$ and determined from the 2nd and 98th percentiles of the height data, shown as a function of time. Error bars were estimated from the standard error of R_a obtained from 5 horizontal equidistant segments of an AFM height image.

× 30 μm area of HKUST-1 thin film in its pristine state (a), and when exposed to humidified nitrogen for 3 h (b), 10 h (c) and 60 h (d) (see Figure S2 for the remaining time steps). We find that after 10 h of exposure to high humidity, the morphology of the surface begins to change significantly, marked by the formation of large crystals that partially cover the surface, and by the formation of cracks that intensify over the course of the experiment. We quantify these water-induced changes in morphology by plotting the roughness of the surface R_a as a function of time (Figure 2e). The roughness R_a increases from initially ≈10 to 60 nm over the course of the experiment.

Next, we tracked individual HKUST-1 crystals within a smaller 3.5 μm × 3.5 μm spot, as shown in Figure 3a–d, see Figure S3 for the remaining time steps. At this smaller scale,

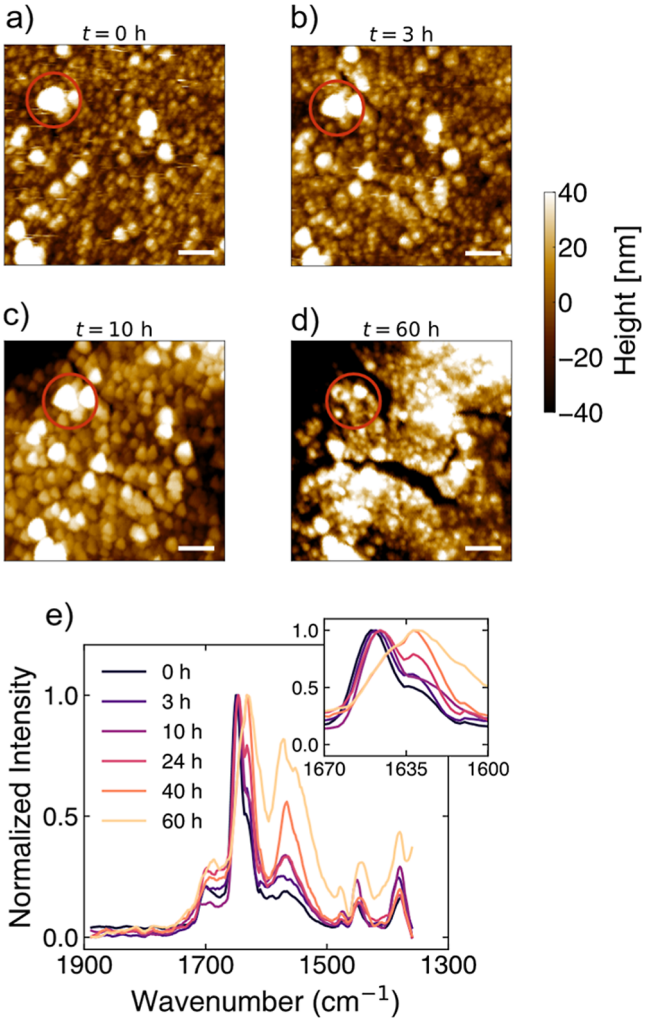

Figure 3. (a–d) AFM height images of HKUST-1 thin film in the pristine state, and after exposure to humidified N_2 for 3 h, 10 and 60 h, respectively. Scale bars are 500 nm. (e) The spectral evolution of a single crystal (highlighted by red circles in the AFM images) at different time steps. The inset shows the spectral region between 1600 and 1670 cm^{-1}.

single crystals showing distinct faceting are clearly visible, as previously observed,[41,42] and the film exhibits faint crack formation as early as 3 h into the experiment (Figures 3b and S3). The cracks, initially ~0.1 μm wide, increase by a factor of ~3 during the duration of the experiment (Figures 3d and S2). We note that given the nominal tip radius of 20 nm, tip convolution tends to overestimate the boundaries of the crystals, which will soften the transition between the crystals. However, the crystals remain discernible in the AFM height images, even after 60 h of exposure to water vapor. Within the area depicted in Figure 3, 9 individual crystals with an average diameter of 200 ± 80 nm were selected and their spectra recorded at discrete time points throughout the water vapor-induced degradation process. Since the crystals fall below the diffraction limit, only techniques that overcome this limit, e.g. AFM-IR can be used for the spectral evaluation of single HKUST-1 thin film crystals. Figure 3e shows the spectral evolution of one of the single crystals investigated (see Figure S4 for the remaining crystals). We note that the signal obtained by AFM-IR is directly proportional to the infrared absorption, as demonstrated by Dazzi and co-workers.[35,36] Initially, at t = 0

https://doi.org/10.1021/acs.jpcc.5c03355
J. Phys. Chem. C 2025, 129, 16617−16623

h, we find all key spectral features of pristine HKUST-1 in the range between 1300 cm^{-1} and 1900 cm^{1} measured here. That includes the peak at 1650 cm^{-1}, which arises from an aromatic CC-stretch mode mixed with an asymmetric COO-stretch mode. The band at 1370 cm^{-1} can be assigned to symmetric COO stretching and the one at 1450 cm^{-1} is an aromatic CC-stretch mode.[23] Upon exposure to humidity, we observe drastic spectral changes within the single crystal measured over time, alluding to its degradation. First, the mixed mode at 1650 cm^{-1} gradually shifts to 1642 cm^{-1}. This shift can be attributed to a lower force constant of the C−O bond caused by H-bonding between the carbonyls and sorbed water molecules.[23] The increase of the band at ≈ 1570 cm^{1} can be assigned to chemisorbed water on defect Cu sites.[23] Most notably, we observe the emergence of a new peak at 1630 cm^{-1} (inset of Figure 3e),[20,43] which was assigned to have the same vibrational nature as the peak observed at 1650 cm^{-1},[23] and is thus suspected to be a COO-stretch mode influenced by hydrogen bonding due to coordinated water molecules. We corroborate this by degrading a different sample of HKUST-1 film using D_2O instead. In this case the peak persists, thereby excluding any contribution from OH bending (Figure S5). The peak at 1705 cm^{-1} can be associated with the protonated carbonyl stretching vibration,[23] i.e. alluding to noncoordinated BTC linker molecules. We observe an overall increase in the band at 1705 cm^{-1} with time, but exclude it from further analysis, because it lies exactly at the transition points between two diodes of the QCL employed, which can give rise to artifacts.[44]

To study the dynamics governing the degradation process, we decided to use the ratio between the intensity of the emerging peak at 1630 cm^{-1} and the maximum peak ∼1650 cm^{-1}, as a probe for the kinetics of the degradation progress within the crystals exposed to humidified N_2. Figure 4a shows a plot of the intensity ratio $\frac{I_{1630cm^{-1}}}{I_{1650cm^{-1}}}$ versus time.

For each individual crystal tracked over a period of 60 h, we model the dynamics of HKUST-1 based on a first-order reaction, fitting a monoexponential function starting from $t = 0$ h and asymptotically approaching the saturation value at t_{max}. Using both the time constant and saturation value as fitting parameters describes our data well. A monoexponential fit to the mean spectral ratios across all crystals studied yields an overall time constant ≈19 h. On the single crystal level, we observe that not only the time constant, but also the extent of HKUST-1 degradation, i.e. the net change in intensity ratio $\Delta\left(\frac{I_{1630cm^{-1}}}{I_{1650cm^{-1}}}\right)$ between t_{max} and $t = 0$ h varies significantly depending on the crystal inspected. Comparing the 1σ errors bars of both time constants and change in intensity ratio indicates heterogeneity in the progress of water-induced HKUST-1 degradation on the single crystal level (Figure S6). A comparison plot of the pristine and degraded spectrum of the crystals with lowest and highest time constant exemplifies this heterogeneity in net degradation over the course of the experiment (Figures 4b and S4): Crystal No. 1 shows extensive degradation while the spectrum of crystal No. 5 changed to a much lower extent after 60 h exposure to humidified N_2.

To further investigate this heterogeneity, we extracted both crystal size and crystal position from the AFM-height maps. For the 9 individual crystals measured here we found no clear correlation between time constant and relative change in framework degradation with crystal size or relative position (Figure S7). Eventually, plotting the surface roughness R_a of the smaller the smaller 3.5 μm × 3.5 μm spot versus $\frac{I_{1630cm^{-1}}}{I_{1650cm^{-1}}}$ reveals a strong correlation, highlighting that the water-induced framework collapse leads to changes in morphology of the MOF thin film morphology (Figure 5). The influence of tip convolution on R_a should be negligible given that the size of the crystals investigated exceeds the radius of the tip used.

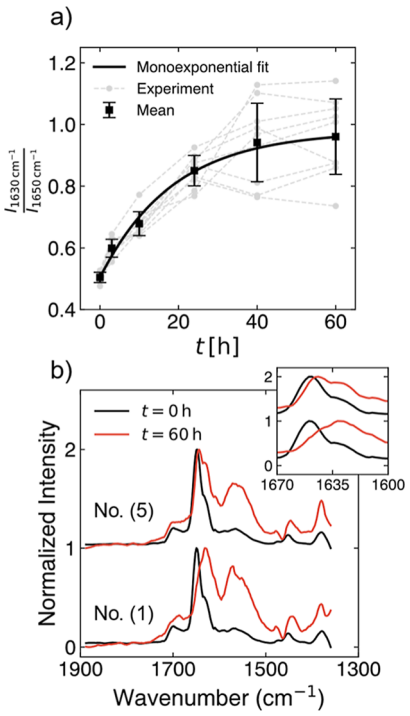

Figure 4. (a) Dynamics of the degradation of single HKUST-1 thin film crystals probed by using the ratio of the peak intensities $\frac{I_{1630cm^{-1}}}{I_{1650cm^{-1}}}$. The data were fit using a monoexponential function with the time constant and the saturation value as free parameters. The solid line shows a fit of the mean ratio from all studied crystals with an overall time constant ≈19 h. (b) AFM-IR spectra of the two pristine and degraded single HKUST-1 crystals of highest and lowest τ with ≈53 h (Crystal No. 1) and ≈7 h (Crystal No. 5), respectively (see their position in Figure S3). The inset shows the spectral region between 1600 and 1670 cm^{-1}.

We infer that this change in MOF thin film morphology, primarily crack formation, as reflected by an increase in R_a within the smaller 3.5 μm × 3.5 μm spot, commences as follows. Exposure to water vapor transforms the thin film of HKUST-1 into $[Cu_2(OH)(BTC)(H_2O)]_n{\cdot}2nH_2O]$. The open, porous cubic structure of HKUST-1 with a unit cell volume of 17.6 nm^3 shrinks to form the much denser monoclinic hydrate, whose unit cell volume is only ≈0.6 nm^3.[39] Given that no material is removed or added to the thin film (except humidified N_2), the increase in framework density causes mechanical stress on the thin film inducing the observed cracks.[45] The transformation of HKUST-1 into $[Cu_2(OH)(BTC)(H_2O)]_n{\cdot}2nH_2O]$ is clearly to be separated from the surface barrier phenomenon. In the case of surface barriers, mass transfer rates are significantly compromised while crystallinity of the MOF thin film remains intact as shown by XRD patterns that are only minimally affected by water vapor.[18,19,24] The extent of MOF thin film degradation appears

https://doi.org/10.1021/acs.jpcc.5c03355
J. Phys. Chem. C 2025, 129, 16617−16623

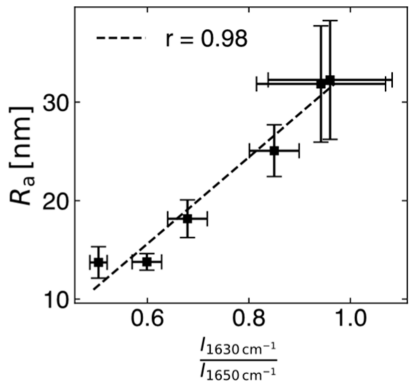

Figure 5. Correlation of the roughness R_a obtained in the spot where spectra of single crystals were taken (at the same position on the sample but at different time steps) with the ratio of the peak intensities $\frac{I_{1630cm}{}^{-1}}{I_{1650cm}{}^{-1}}$ used as a probe for HKUST-1 framework collapse. The data reveal a positive correlation (Pearson's r = 0.98, defined as $\frac{\sum_{i=1}^{n}(x_i-\bar{x})(y_i-\bar{y})}{\sqrt{\sum_{i=1}^{n}(x_i-\bar{x})^2}\sqrt{\sum_{i=1}^{n}(y_i-\bar{y})^2}}$, with x the ratio of the intensities and y the roughness).

to be affected by humidity and exposure time to water vapor: HKUST-1 degradation is observed to go beyond the mere formation of surface defects toward transformation to $[Cu_2(OH)(BTC)(H_2O)]_n{\cdot}2nH_2O]$ when relative humidity and exposure time increase. Any morphological changes, along with the spectral shifts reported here are a clear indication of the transformation of HKUST-1. We note that these findings are uniquely enabled by AFM-IR, which provides nanoscale morphological and spectroscopic information in a single measurement.

CONCLUSIONS

A thin film of HKUST-1 exposed to water vapor leads to its degradation and transformation into a much denser hydrated phase. Using atomic force microscopy-infrared spectroscopy we tracked spectral and morphological changes of this transformation locally on the nanoscale. Morphologically, large crystals of the new phase precipitate on the surface accompanied by the formation of cracks, which we conclude to result from the dramatic change in density between the two phases. Spectrally, we monitored the degradation of HKUST-1 using its asymmetric COO stretching, which we found to gradually shift to lower frequencies. The shift can be modeled using first-order kinetics and the data reveal that the transformation of HKUST-1 commences heterogeneously on the single crystal level. Most notably we found a direct correlation between spectral changes indicating framework collapse and changes in surface morphology. Our findings underscore the need to design thin films of MOFs with potential exposure to water vapor in mind. Water-induced degradation not only compromises the framework itself, but also significantly alters the morphology of MOF thin films, which impedes their use in any applications based on loading with guest molecules. These insights contribute to a deeper understanding of the environmental stability of MOF thin films, which is critical for integration into real-world devices. Control over humidity-induced degradation mechanisms enables the development of more robust, humidity-tolerant MOF-based coatings and sensors. Future work could involve different types of MOFs, monitoring the crack formation more dynamically or investigating how the kinetics of the transformation of the crystals are affected by tuning humidity values or flow parameters.

ASSOCIATED CONTENT

Supporting Information

The Supporting Information is available free of charge at https://pubs.acs.org/doi/10.1021/acs.jpcc.5c03355.

Determine Sample Thickness, AFM Height Maps, AFM-IR Spectra of Single Crystals, D_2O Reference Measurement, HKUST-1 Degradation as a Function of Crystal Size and Position (PDF)

AUTHOR INFORMATION

Corresponding Author

Marius R. Bittermann − *Institute of Chemistry and Biochemistry, Freie Universität Berlin, Berlin 14195, Germany*; orcid.org/0000-0001-6399-4469; Email: m.bittermann@fu-berlin.de

Authors

Sudheer Singh Rana − *Institute of Chemistry and Biochemistry, Freie Universität Berlin, Berlin 14195, Germany*

Michael Tovar − *Abteilung Struktur und Dynamiken von Energiematerialien, Helmholtz Zentrum Berlin, Berlin 14109, Germany*

Lars Heinke − *Institute of Chemistry and Biochemistry, Freie Universität Berlin, Berlin 14195, Germany*; orcid.org/0000-0002-1439-9695

Complete contact information is available at: https://pubs.acs.org/10.1021/acs.jpcc.5c03355

Author Contributions

M. R. B conceived the experiments, conducted AFM-IR measurements, data analysis, writing the first draft. M. T. & S. S. R. conducted XRD measurements. L. H. conceived the experiments. All authors reviewed and approved the final manuscript.

Notes

The authors declare no competing financial interest.

REFERENCES

(1) Furukawa, H.; Cordova, K. E.; O'Keeffe, M.; Yaghi, O. M. The chemistry and applications of metal-organic frameworks. *Science* **2013**, *341* (6149), 1230444.

(2) Zhou, H. C. J.; Kitagawa, S. Metal−organic frameworks (MOFs). *Chem. Soc. Rev.* **2014**, *43* (16), 5415−5418.

(3) Li, H.; Eddaoudi, M.; O'Keeffe, M.; Yaghi, O. M. Design and synthesis of an exceptionally stable and highly porous metal-organic framework. *Nature* **1999**, *402* (6759), 276−279.

(4) Jiao, L.; Wang, Y.; Jiang, H. L.; Xu, Q. Metal−organic frameworks as platforms for catalytic applications. *Adv. Mater.* **2018**, *30* (37), 1703663.

(5) He, B.; Zhang, Q.; Pan, Z.; Li, L.; Li, C.; Ling, Y.; Wang, Z.; Chen, M.; Wang, Z.; Yao, Y.; et al. Freestanding metal−organic frameworks and their derivatives: an emerging platform for electrochemical energy storage and conversion. *Chem. Rev.* **2022**, *122* (11), 10087−10125.

(6) Zhou, X.; Jin, H.; Xia, B. Y.; Davey, K.; Zheng, Y.; Qiao, S. Z. Molecular cleavage of metal-organic frameworks and application to energy storage and conversion. *Adv. Mater.* **2021**, *33* (51), 2104341.

(7) Jia, T.; Gu, Y.; Li, F. Progress and potential of metal-organic frameworks (MOFs) for gas storage and separation: A review. *J. Environ. Chem. Eng.* **2022**, *10* (5), 108300.
(8) Li, H.; Wang, K.; Sun, Y.; Lollar, C. T.; Li, J.; Zhou, H.-C. Recent advances in gas storage and separation using metal−organic frameworks. *Mater. Today* **2018**, *21* (2), 108−121.
(9) Shu, Y.; Ye, Q.; Dai, T.; Xu, Q.; Hu, X. Encapsulation of luminescent guests to construct luminescent metal−organic frameworks for chemical sensing. *ACS Sensors* **2021**, *6* (3), 641−658.
(10) Yassine, O.; Shekhah, O.; Assen, A. H.; Belmabkhout, Y.; Salama, K. N.; Eddaoudi, M. H_2S sensors: fumarate-based fcu-MOF thin film grown on a capacitive interdigitated electrode. *Angew. Chem.* **2016**, *128* (51), 16111−16115.
(11) Horcajada, P.; Gref, R.; Baati, T.; Allan, P. K.; Maurin, G.; Couvreur, P.; Férey, G.; Morris, R. E.; Serre, C. Metal−organic frameworks in biomedicine. *Chem. Rev.* **2012**, *112* (2), 1232−1268.
(12) Rabiee, N.; Atarod, M.; Tavakolizadeh, M.; Asgari, S.; Rezaei, M.; Akhavan, O.; Pourjavadi, A.; Jouyandeh, M.; Lima, E. C.; Hamed Mashhadzadeh, A.; et al. Green metal-organic frameworks (MOFs) for biomedical applications. *Microporous Mesoporous Mater.* **2022**, *335*, 111670.
(13) Yang, L.; Wang, K.; Guo, L.; Hu, X.; Zhou, M. Unveiling the potential of HKUST-1: synthesis, activation, advantages and biomedical applications. *J. Mater. Chem. B* **2024**, *12* (11), 2670−2690.
(14) Ding, M.; Cai, X.; Jiang, H.-L. Improving MOF stability: approaches and applications. *Chem. Sci.* **2019**, *10* (44), 10209−10230.
(15) Burtch, N. C.; Jasuja, H.; Walton, K. S. Water stability and adsorption in metal−organic frameworks. *Chem. Rev.* **2014**, *114* (20), 10575−10612.
(16) Canivet, J.; Fateeva, A.; Guo, Y.; Coasne, B.; Farrusseng, D. Water adsorption in MOFs: fundamentals and applications. *Chem. Soc. Rev.* **2014**, *43* (16), 5594−5617.
(17) Chui, S. S.-Y.; Lo, S. M.-F.; Charmant, J. P.; Orpen, A. G.; Williams, I. D. A chemically functionalizable nanoporous material $[Cu_3(TMA)_2(H_2O)_3]_n$. *Science* **1999**, *283* (5405), 1148−1150.
(18) Heinke, L.; Gu, Z.; Wöll, C. The surface barrier phenomenon at the loading of metal-organic frameworks. *Nat. Commun.* **2014**, *5* (1), 4562.
(19) Müller, K.; Vankova, N.; Schöttner, L.; Heine, T.; Heinke, L. Dissolving uptake-hindering surface defects in metal−organic frameworks. *Chem. Sci.* **2019**, *10* (1), 153−160.
(20) DeCoste, J. B.; Peterson, G. W.; Schindler, B. J.; Killops, K. L.; Browe, M. A.; Mahle, J. J. The effect of water adsorption on the structure of the carboxylate containing metal−organic frameworks Cu-BTC, Mg-MOF-74, and UiO-66. *J. Mater. Chem. A* **2013**, *1* (38), 11922−11932.
(21) Domán, A.; Czakkel, O.; Porcar, L.; Madarász, J.; Geissler, E.; László, K. Role of water molecules in the decomposition of HKUST-1: Evidence from adsorption, thermoanalytical, X-ray and neutron scattering measurements. *Appl. Surf. Sci.* **2019**, *480*, 138−147.
(22) Majano, G.; Martin, O.; Hammes, M.; Smeets, S.; Baerlocher, C.; Pérez-Ramírez, J. Solvent-Mediated Reconstruction of the Metal−Organic Framework HKUST-1 $(Cu_3(BTC)_2)$. *Adv. Funct. Mater.* **2014**, *24* (25), 3855−3865.
(23) Gentile, F. S.; Pannico, M.; Causa, M.; Mensitieri, G.; Di Palma, G.; Scherillo, G.; Musto, P. Metal defects in HKUST-1 MOF revealed by vibrational spectroscopy: A combined quantum mechanical and experimental study. *J. Mater. Chem. A* **2020**, *8* (21), 10796−10812.
(24) Li, C.; Chandresh, A.; Zhang, Z.; Moulai, S.; Heinke, L. Stability and Degradation of Metal−Organic-Framework Films under Ambient Air Explored by Uptake and Diffusion Experiments. *Adv. Mater. Interfaces* **2022**, *9* (3), 2101947.
(25) Loera-Serna, S.; Beltrán, H. I.; Mendoza-Sánchez, M.; Álvarez-Zeferino, J. C.; Almanza, F.; Fernández-Luqueño, F. Effect of HKUST-1 metal−organic framework in root and shoot systems, as well as seed germination. *Environ. Sci. Pollut. Res.* **2024**, *31* (9), 13270−13283.
(26) Rodríguez-Esteban, C.; Ayala, R.; López-Cartes, C. Stability and performance of BTC-based MOFs for environmental applications. *J. Solid State Chem.* **2024**, *339*, 124956.
(27) Shekhah, O.; Wang, H.; Kowarik, S.; Schreiber, F.; Paulus, M.; Tolan, M.; Sternemann, C.; Evers, F.; Zacher, D.; Fischer, R. A.; et al. Step-by-step route for the synthesis of metal−organic frameworks. *J. Am. Chem. Soc.* **2007**, *129* (49), 15118−15119.
(28) Marshall, C. R.; Staudhammer, S. A.; Brozek, C. K. Size control over metal−organic framework porous nanocrystals. *Chem. Sci.* **2019**, *10* (41), 9396−9408.
(29) Rivera-Torrente, M.; Mandemaker, L. D.; Filez, M.; Delen, G.; Seoane, B.; Meirer, F.; Weckhuysen, B. M. Spectroscopy, microscopy, diffraction and scattering of archetypal MOFs: formation, metal sites in catalysis and thin films. *Chem. Soc. Rev.* **2020**, *49* (18), 6694−6732.
(30) Delen, G.; Monai, M.; Stančiaková, K.; Baumgartner, B.; Meirer, F.; Weckhuysen, B. M. Structure sensitivity in gas sorption and conversion on metal-organic frameworks. *Nat. Commun.* **2023**, *14* (1), 129.
(31) Mandemaker, L. D.; Filez, M.; Delen, G.; Tan, H.; Zhang, X.; Lohse, D.; Weckhuysen, B. M. Time-resolved in situ liquid-phase atomic force microscopy and infrared nanospectroscopy during the formation of metal−organic framework thin films. *J. Phys. Chem. Lett.* **2018**, *9* (8), 1838−1844.
(32) Shu, D.; Fan, R.; Yao, S.; Jiang, H.; Zhang, X.; Zheng, Y. Electrical and Mechanical Controllability of Rotor Dynamics in MOF Thin Films Revealed by AFM-IR. *J. Phys. Chem. C* **2024**, *128* (30), 12551−12557.
(33) Delen, G.; Monai, M.; Meirer, F.; Weckhuysen, B. M. In situ nanoscale infrared spectroscopy of water adsorption on nanoislands of surface-anchored metal-organic frameworks. *Angew. Chem., Int. Ed.* **2021**, *60* (3), 1620−1624.
(34) Moslein, A. F.; Donà, L.; Civalleri, B.; Tan, J.-C. Defect engineering in metal−organic framework nanocrystals: Implications for mechanical properties and performance. *ACS Appl. Nano Mater.* **2022**, *5* (5), 6398−6409.
(35) Dazzi, A.; Prater, C. B. AFM-IR: Technology and applications in nanoscale infrared spectroscopy and chemical imaging. *Chem. Rev.* **2017**, *117* (7), 5146−5173.
(36) Dazzi, A.; Prazeres, R.; Glotin, F.; Ortega, J. Local infrared microspectroscopy with subwavelength spatial resolution with an atomic force microscope tip used as a photothermal sensor. *Opt. Lett.* **2005**, *30* (18), 2388−2390.
(37) Gu, Z.-G.; Pfriem, A.; Hamsch, S.; Breitwieser, H.; Wohlgemuth, J.; Heinke, L.; Gliemann, H.; Wöll, C. Transparent films of metal-organic frameworks for optical applications. *Microporous Mesoporous Mater.* **2015**, *211*, 82−87.
(38) Müller, K.; Singh Malhi, J.; Wohlgemuth, J.; Fischer, R. A.; Wöll, C.; Gliemann, H.; Heinke, L. Water as a modulator in the synthesis of surface-mounted metal−organic framework films of type HKUST-1. *Dalton Trans.* **2018**, *47* (46), 16474−16479.
(39) Chen, J.; Yu, T.; Chen, Z.; Xiao, H.; Zhou, G.; Weng, L.; Tu, B.; Zhao, D. Synthesis and Structure of a New 3D Porous Cu(II)−Benzene-1, 3, 5-tricarboxylate Coordination Polymer,$[Cu_2(OH)(BTC)(H_2O)]_n \cdot 2nH_2O$. *Chem. Lett.* **2003**, *32* (7), 590−591.
(40) Seo, Y.-K.; Hundal, G.; Jang, I. T.; Hwang, Y. K.; Jun, C.-H.; Chang, J.-S. Microwave synthesis of hybrid inorganic−organic materials including porous $Cu_3(BTC)_2$ from Cu(II)-trimesate mixture. *Microporous Mesoporous Mater.* **2009**, *119* (1−3), 331−337.
(41) Summerfield, A.; Cebula, I.; Schröder, M.; Beton, P. H. Nucleation and early stages of layer-by-layer growth of metal organic frameworks on surfaces. *J. Phys. Chem. C* **2015**, *119* (41), 23544−23551.
(42) Ohnsorg, M. L.; Beaudoin, C. K.; Anderson, M. E. Fundamentals of MOF thin film growth via liquid-phase epitaxy: investigating the initiation of deposition and the influence of temperature. *Langmuir* **2015**, *31* (22), 6114−6121.
(43) Abou-Elyazed, A. S.; Ftooh, A. I.; Sun, Y.; Ashry, A. G.; Shaban, A. K.; El-Nahas, A. M.; Yousif, A. M. Solvent-Free Synthesis of HKUST-1 with Abundant Defect Sites and Its Catalytic Performance

in the Esterification Reaction of Oleic Acid. *ACS Omega* **2024**, *9* (36), 37662−37671.
(44) Schwartz, J. J.; Jakob, D. S.; Centrone, A. A guide to nanoscale IR spectroscopy: resonance enhanced transduction in contact and tapping mode AFM-IR. *Chem. Soc. Rev.* **2022**, *51* (13), 5248−5267.
(45) Liu, M.; Yu, S.; He, L.; Ni, Y. Recent progress on crack pattern formation in thin films. *Soft Matter* **2022**, *18* (32), 5906−5927.

https://doi.org/10.1021/acs.jpcc.5c03355
J. Phys. Chem. C 2025, 129, 16617−16623